Electronic Supplementary Information for

Boosting CO_2 electroreduction on a Zn electrode via concurrent surface reconstruction and interfacial surfactant modification

Hui Pan,[a] Fang Wang,[a] Shixiong She,[b] Zhengguo Zhang[a] and Shixiong Min*[a]

[a] *School of Chemistry and Chemical Engineering, North Minzu University, Yinchuan, 750021, P. R. China.*

[b] *College of Chemical Engineering, Qinghai University, Xining 810016, P. R. China.*

*Corresponding authors: sxmin@nun.edu.cn

1. Experimental

1.1 Chemicals and reagents

All chemicals used in this work were of analytical grade and used without further purification. Zinc foil (99.99%, thickness: 0.3 mm) was purchased from Tengfeng Metal Materials Co., Ltd. Cetyltrimethylammonium bromide (CTAB, 99%) and Potassium bicarbonate ($KHCO_3$, 99.5%) were obtained from Aladdin Industrial Co., Ltd. The CO_2 (99.999%) and N_2 was purchased from Jinghua Industrial Gas Co., Ltd. Nafion 117 membrane was provided by Alfa Aesar Chemical Co., Ltd. Ultrapure water (18.2 MΩ cm) obtained from a water purification system (Hitech ECO-S15) was used in all experiments. The pH value of the electrolyte saturated with CO_2 was determined to be 6.8.

1.2 Synthesis of annealed Zn electrodes

A piece of zinc foil (1.0 cm×1.5 cm) was mechanically polished with sandpaper (2000 mesh) to remove the natural oxide layer, and then successively washed with acetone, water, and ethanol, and finally dried under a flow of N_2 at room temperature. Zn foil was annealed in a tubular CVD furnace under static air atmosphere at different temperatures ranging from 400 to 700 °C for 6 h.

1.3 Synthesis of OD-Zn and OD-Zn-CTAB electrodes

OD-Zn and OD-Zn-CTAB electrodes were obtained by in situ electrochemical reduction of annealed Zn electrodes in CO_2-saturated 0.1 M $KHCO_3$ electrolyte without and with addition of CTAB (50 μM) at -0.8 V *vs*. RHE for 1 h, respectively.

1.4 Electrochemical measurements

The electrochemical CO_2 reduction experiments were performed in a H-type cell separated by a Nafion 117 membrane with a CHI660E electrochemical workstation (CH Instruments, Inc., Shanghai). An Ag/AgCl (in a saturated KCl solution) and a Pt coil

were used as the reference electrode and the counter electrode, respectively, and CO_2-saturated 0.1 M $KHCO_3$ (pH 6.8) was used as electrolyte. All the applied potentials were reported as revisable hydrogen electrode (RHE) potentials scale using *E* (*vs*. RHE) =*E* (*vs.* Ag/AgCl)+0.656 V–iR_s. The reference electrode was calibrated with a Pt coil as the working electrode for the reversible hydrogen potential in the electrolyte solution purged with N_2 for 30 min and saturated high purity H_2 prior to the measurements. The cyclic voltammetry (CV) was run at a scan rate of 1 mV s^{-1}, and the average of the two potentials at which the current crossed zero was taken to be the thermodynamic potential for the hydrogen electrode reactions.[1] Liner sweep voltammetry (LSV) measurements for the electrodes was carried out in were performed N_2- or CO_2-bubbled 0.1 M $KHCO_3$ solution with a scan rate of 1 mV s^{-1}. For the bulk CO_2 electrolysis, the cathodic compartment was purged with CO_2 (99.999%) at a constant rate of 10 mL min^{-1}. The eluent was delivered directly to the sampling loop of an on-line pre-calibrated gas chromatograph (PANNA GC-A91 plus) equipped with a thermal conductivity detector (TCD) and a flame ionization detector (FID). Faradaic efficiency (FE) of gaseous products at each applied potential was calculated based on following equation:

$$FE_i(\%) = \frac{Z_i \times G \times V_i \times t \times p_0 \times F \times 10^{-3}}{Q_{total} \times R \times T_0} \times 100\%$$

where Z_i is the number of electrons transferred (for CO and H_2 production; Z=2); G is volumetric flow rate (10 mL min^{-1}); V_i is the volume ratio of gas product i; t is reaction time (min); P_0 and T_0 are atmospheric pressure (101.3 KPa) and reaction temperature (298.15 K); respectively. F is faradaic constant (96485 C mol^{-1}); Q_{total} is integrated charge at each applied potential and R is ideal gas constant (8.314 J·mol^{-1} K^{-1}).

At the end of the electrolysis, the produced liquid phase products were detected by

using a high-performance liquid chromatography (HPLC, Hitachi) system equipped with C18 column and UV detector. A mixture of methanol (10 %) and phosphoric acid (pH 2) was used as the mobile phase at 25 ^{o}C with a continuous flow rate of 0.6 mL min^{-1}.

1.5 Electrochemical impedance spectroscopy measurements

Electrochemical impedance measurements were performed in CO_2-saturated 0.1 M $KHCO_3$ electrolytes in the absence or presence of CTAB at different polarization potentials. Within the frequency range between 10^5 Hz and 0.01 Hz and 5 mV amplitude. We used the equivalent circuit of Fig. 4b to simulate the experimental data points. Double layer capacitances were calculated using the equation, where *R*s is the solution resistance, R_{ct} is the charge transfer resistance, CPE is the constant phase element, n is the fitting parameter which was also found after the fitting of the Nyquist plots. Double layer capacitance (C_{dl}) value has been calculated using the equation as follows:

$$C_{dl} = \left\{R_{CT}{}^{(1-N)} CPE\right\}^{(1/N)}$$

1.6 Determination of the electrochemically active surface areas (ECSAs)

Cyclic voltammetry (CV) tests were performed in CO_2-purged 0.05 M $K_3[Fe[(CN)_6]$ solution (0.1 M $KHCO_3$ as supporting electrolyte) to determine the electrochemically active surface areas (ECSAs) of the all samples.[2-3] In this system, the relationship between the peak current value [(i_{pc}+i_{pa})/2] and the square root of the potential scanning velocity ($v^{1/2}$) can be described by the Randles-Sevcik equation:

$$i_p = 2.69 \times 10^5 n^{3/2} A D^{1/2} v^{1/2} C$$

where i_p is the peak current value (A); *n* is the number of electron transfer; *A* is the ESCA of the electrode (cm^2); *D* is the diffusion coefficient (cm^2 s^{-1}); *C* is the concentration of $K_3[Fe[(CN)_6]$ (mol cm^{-3}); v is the scanning speed (V s^{-1}).

1.7 Characterizations

X-ray powder diffraction (XRD) was performed with a Rigaku smart lab diffractometer operated at 40 kV and 40 mA with nickel filtrated Cu *K*α radiation. X-ray photoelectron spectroscopy (XPS) analysis were performed using Thermos Scientific ESCALAB 250Xi instrument. The instrument was equipped with an electron flood and a scanning ion gun. All spectra were calibrated according to the C 1s binding energy at 284.8 eV. Scanning electron microscopy (SEM) and energy X-ray spectrometer (EDS) were performed using a field emission microscope (SIGMA 500) for analyze the morphology and composition of the catalyst.

2. Additional data

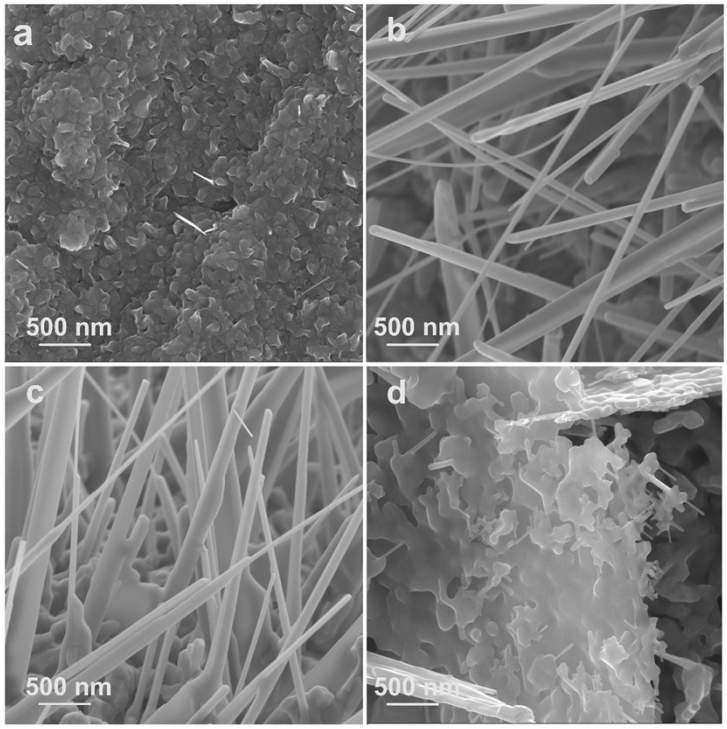

Fig. S1 SEM images of annealed Zn electrodes prepared by annealing Zn foil at (a) 400 °C, (b) 500 °C, (c) 600 °C and (d) 700 °C.

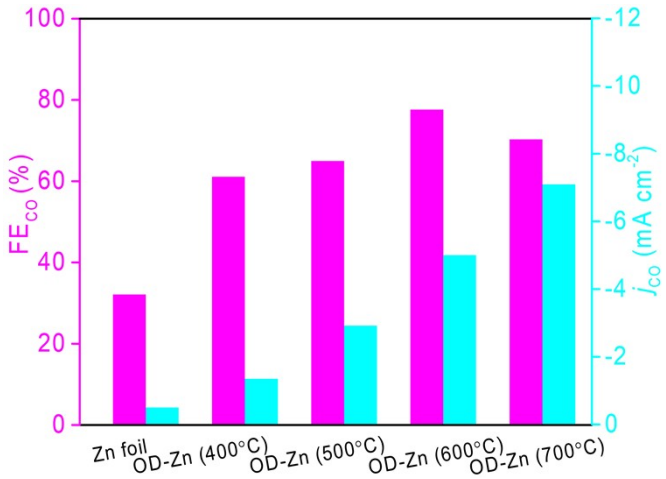

Fig. S2 FE_{CO} and j_{CO} for Zn foil and OD-Zn electrodes in CO_2-saturated 0.1 M $KHCO_3$ electrolyte.

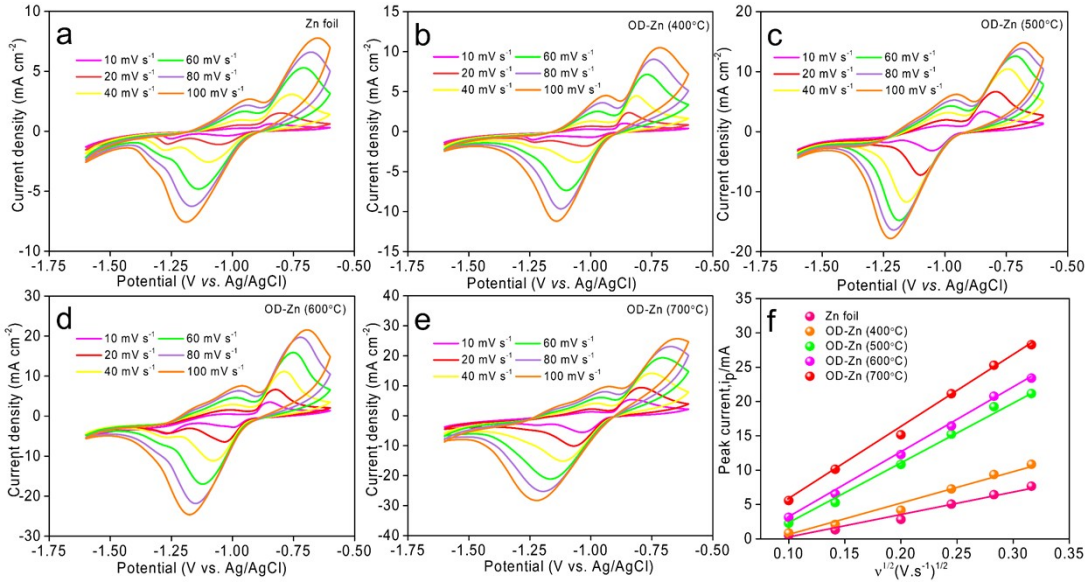

Fig. S3 Cyclic voltammograms (CV) of (a) pristine Zn foil and (b-e) OD-Zn electrodes at different scan rates. (f) The curves of the peak current ($(i_{pc}+i_{pa})/2$) as a function of square root of the scan rate ($v^{1/2}$) of all samples.

Table S1 Electrochemical active surface areas (ECSAs) of pristine Zn foil and OD-Zn electrodes.

Electrode	ECSA (cm^2)
Zn foil	1.02
OD-Zn (400 °C)	1.43
OD-Zn (500 °C)	2.72
OD-Zn (600 °C)	2.85
OD-Zn (700 °C)	3.17

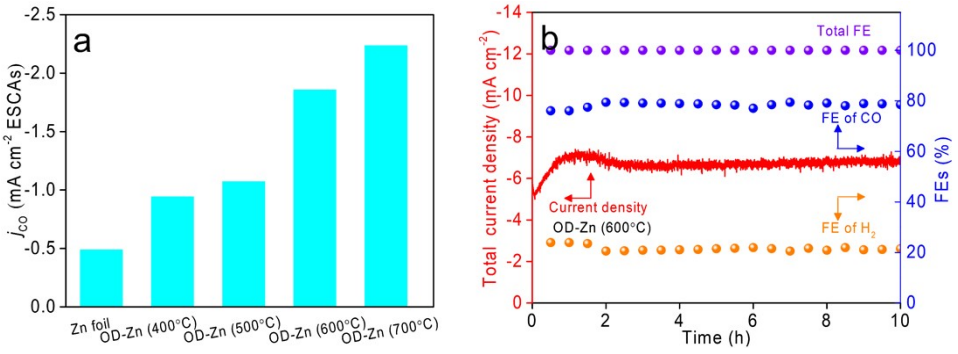

Fig.S4 (a) ECSA-normalized j_{CO} of pristine Zn foil and OD-Zn electrodes. (b) Electrocatalytic stability of OD-Zn (600 °C) electrode for CO_2 reduction in CO_2-saturated 0.1 M $KHCO_3$ at -1.0 V *vs*. RHE over a period of 10 h.

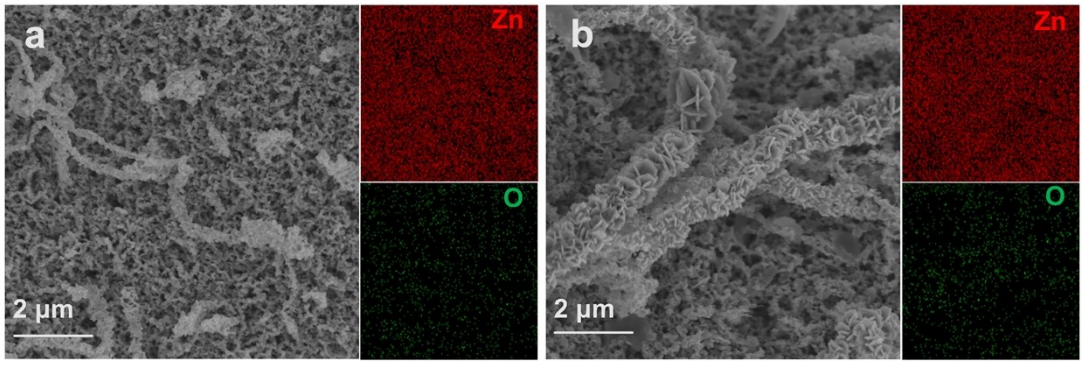

Fig. S5 SEM images of OD-Zn and OD-Zn-CTAB electrodes and the corresponding elemental maps (Zn and O).

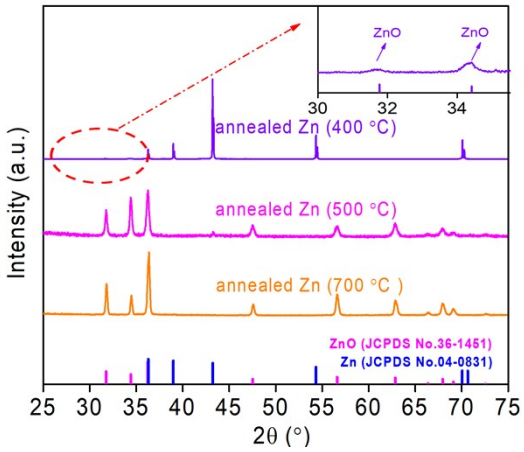

Fig. S6 XRD patterns of annealed Zn electrodes.

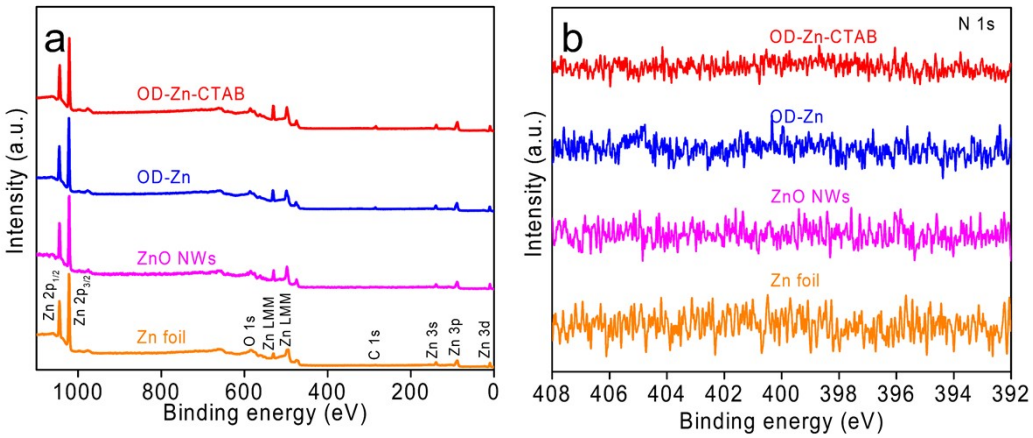

Fig. S7 Survey and N 1s XPS spectrum and of Zn foil, ZnO NWs, OD-Zn and OD-Zn-CTAB

Table S2 Comparison of electrocatalytic performances of Zn-based catalysts for CO_2 reduction.

Catalysts	Electrolyte	Potential (V *vs.* RHE)	j_{CO} (mA cm^{-2})	FE_{CO}	Overpotential for CO_2 reduction	Ref.
Porous nanostructured Zn	0.5 M $KHCO_3$	-0.9	~6.6	77.8%	0.79	4
Zn/carbon/Ag	0.5 M $KHCO_3$	-1.0	~7.3	86%	0.89	5
Multilayered Zn nanosheets	0.5 M $NaHCO_3$	-1.13	~7.8	86%	1.02	6
Commercial Zn foil	0.1 M $KHCO_3$	-1.3	~4.1	78.9	1.19	7
Porous Zn	0.1M $KHCO_3$	-0.8	~1.2	81%	0.69	8
Ag nanoparticles decorated Zn nanoplates	0.1 M $KHCO_3$	-0.8	~4.9	84%	0.69	9
Hexagonal Zn nanoplates	0.1 M $KHCO_3$	-0.96	~6	94.2%	0.85	10
ZnS/Zn/ZnS	0.1 M $KHCO_3$	-0.8	~9	94.2%	0.69	11
Nanoscale Zn	0.5 M NaCl	-1.6	~2.2	93%	1.49	12
OD-Zn-CTAB	**0.1M $KHCO_3$ (50M CTAB)**	**-1.0**	**~8.2**	**90%**	**0.89**	**This word**

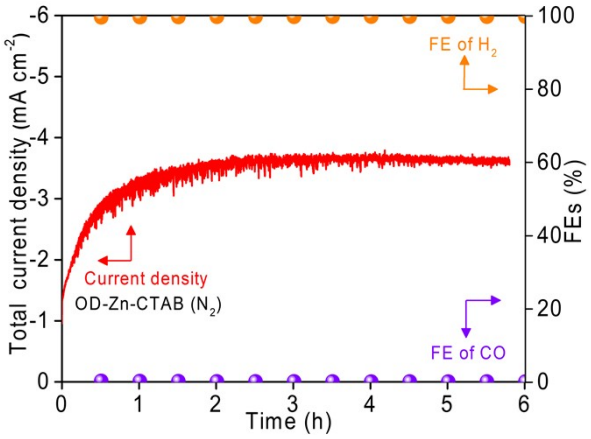

Fig. S8 The total current density and FEs of CO and H_2 over OD-Zn-CTAB electrode in N_2-saturated 0.1 M $KHCO_3$ solution with 50 μM CTAB at -1.0 V *vs*. RHE.

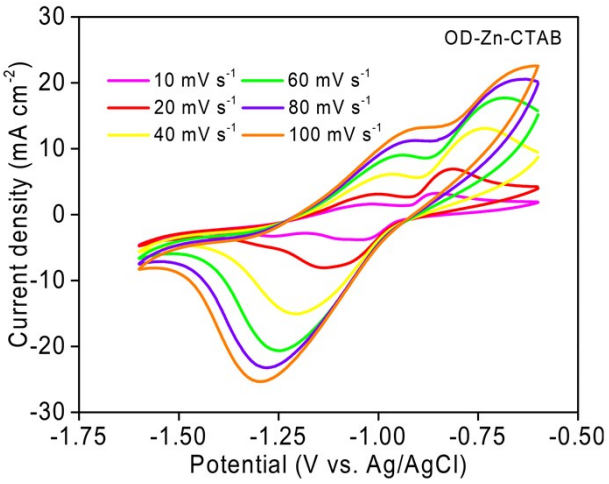

Fig. S9 Cyclic voltammograms (CV) of OD-Zn-CTAB.

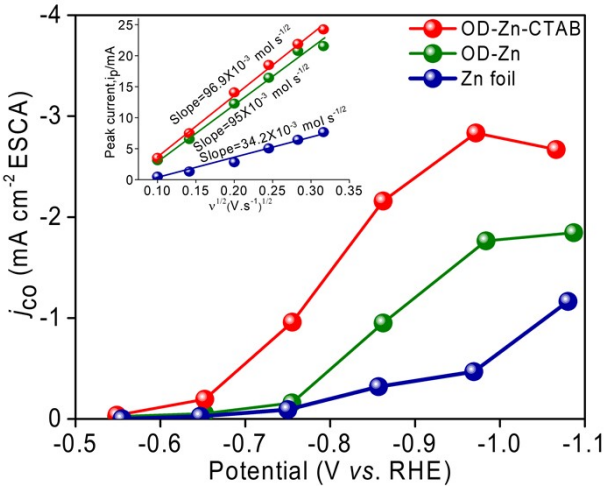

Fig. S10 ECSA-normalized CO current densities of Zn foil, OD-Zn and OD-Zn-CTAB. The insets in panel are the curves of the peak current ($(i_{pc}+i_{pa})/2$) as a function of square root of the scan rate ($v^{1/2}$).

Table S3 Electrochemical active surface areas (ECSAs) of Zn foil, OD-Zn and OD-Zn-CTAB.

Electrode	ECSA (cm^2)
Zn foil	1.02
OD-Zn	2.85
OD-Zn-CTAB	2.89

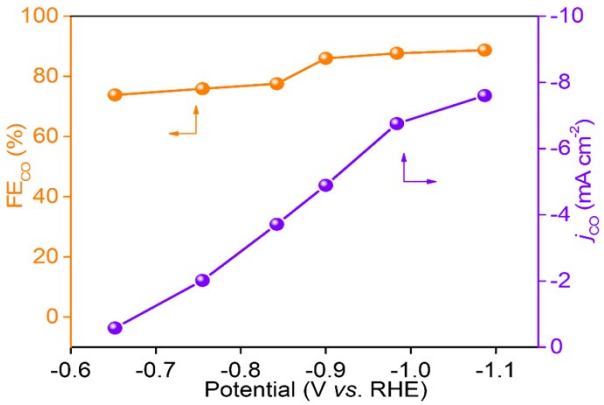

Fig. S11 FE_{CO} and j_{CO} for Zn foil electrode in CO_2-saturated 0.1 M $KHCO_3$ in presence of 50 μM CTAB.

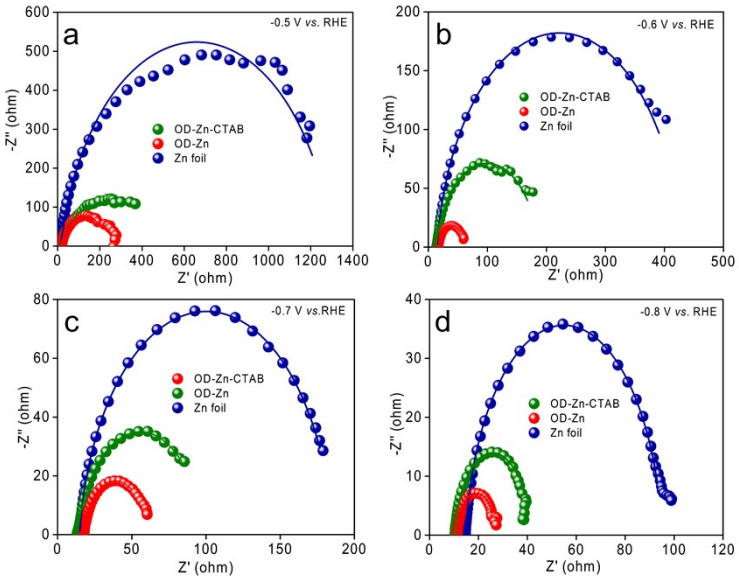

Fig. S12 Nyquist plots of Zn foil, OD-Zn, and OD-Zn-CTAB at different potentials.

Table S4. Simulated impedance parameters of Nyquist plots in variously potentials with and without CTAB.

Catalyst	E (V *vs.* RHE)	R_s (Ω)	R_{CT} (Ω)	C_{dl} (μF cm^{-2})
OD-Zn-CTAB	-0.5	12.7	343.6	344.5
	-0.6	12.8	173.9	293.4
	-0.7	13.0	85.2	293.4
	-0.8	13.2	30.7	223.0
OD-Zn	-0.5	17.3	222.0	2498.0
	-0.6	17.7	43.2	594.5
	-0.7	17.7	43.1	475.5
	-0.8	19.3	15.2	238.3

References

1. S. Banerjee, X. Han and V. S. Thoi, *ACS Catal*., 2019, **9**, 5631-5637.
2. X. L. Cui, Q. Zhao, Z. Z. Li, Z. Y. Sun and Z. Y. Jiang, *Nanotechnology*, 2007, **18**, 215701.
3. H. Pan, F. Wang, Z. G. Zhang and S. X. Min, *Sustainable Energy Fuels*, 2022, **6**, 2149-2154.
4. D. L. Nguyen, M. S. Jee, D. H. Won, H. Jung, H. S. Oh, B. K. Min and Y. J Hwang, *ACS Sustainable Chem. Eng*., 2017, **5**, 11377-11386.
5. F. Yang, P. Song, X. Liu, B. Mei, W. Xing, Z. Jiang, L. Gu and W. Xu, *Angew. Chem. Int. Ed*., 2018, **57**, 12303-12307.
6. T. Zhang, X. Li, Y. Qiu, P. Su, W. Xu, H. Zhong and H. Zhang, *J. Catal*., 2018, **357**, 154-162.
7. Z. Chen, K. Mou, S. Yao and L. Liu, *ChemSusChem*, 2018, **11**, 2944-2952.
8. M. Morimoto, Y. Takatsuji, K. Hirata, T. Fukuma, T. Ohno, T. Sakakura and T. Haruyama, *Electrochim. Acta*, 2018, **290**, 255-261.
9. F. Quan, D. Zhong, H. Song, F. Jia and L. Zhang, *J. Mater. Chem. A*, 2015, **3**, 16409-16413.
10. J. Xiao, M. R. Gao, S. B. Liu, J. L. Luo, *ACS Appl. Mater. Interfaces*, 2020, **12**, 31431-31438.
11. C. Li, G. Shen, R. Zhang, D. Wu, C. Zou, T. Ling, H. Liu, C. Dong and X. W. Du, *J. Mater. Chem. A*, 2019, **7**, 1418-1423.
12. Q. Yu, X. Meng, L. Shi, H. Liu and J. Ye, *Chem. Commun*., 2016, **52**, 14105-14108.